Lightweight Visualisation for Vortex Tracking in Airflow Acquisition

Nicolas Courilleau[1][a], Louis-Wilhelm Raban-Schürmann[1][b], Daniel Meneveaux[1][c],
Kamel Abed-Meraim[2] and Anas Sakout[2][d]

[1]*Université de Poitiers, XLIM Institute, CNRS UMR 7252, France*

[2]*Université de La Rochelle, LaSIE, CNRS UMR 7356, France*

anas.sakout}@univ-lr.fr

Keywords: Visualisation of Airflow, Rendering, Vortex Analysis, Flow Tracking.

Abstract: Ventilation systems are spread in most buildings and housing. They provide control on air quality, while provisioning acceptable thermal conditions. However, slotted plates that direct air jets often produce acoustic disturbances with a self-sustained tone. Understanding and controlling the phenomenon requires complex experimentation with expensive setups. This article proposes an open source, web-based, interactive visualisation system dedicated to the observation and analysis of recorded high frequency captures (3kHz or more) of air streams, charged with thin oil particles. It relies on the acquired images and estimated vector fields, coming from industrial existing systems. Our goal is to visualise the main flow parameters, such as speed, gradients, directions, vortex tracking with path prediction, and vortex frequencies. The obtained results highlight interesting phenomena that illustrate sounds production. They can be employed by physicists to understand, explain, and control the generated acoustics.

1 INTRODUCTION

Airflow control in the industry is widely employed in various contexts such as air conditioning systems, or wind tunnel operations for instance. Unfortunately, the geometric shape of flap systems creates disturbances that often result in undesirable acoustic phenomena, such as whistling or humming. With some configurations, oscillating patterns appear and intensify noise. Countermeasures can be considered, based on flat shapes or flow manipulators. However, setting up an experimental system is costly, requires a rigorously controlled environment, and involves extensive testing.

For these reasons, several authors have conducted comprehensive studies on plane jets with obstacles using PIV (Particle image velocimetry) techniques (Gutmark et al., 1978; Sakakibara et al., 2001). For instance, it has been determined that the detachment frequency of vortex rollers in a plane jet is influenced by the jet's initial conditions (Yokobori et al., 1983).

---

[a] https://orcid.org/0000-0001-7707-9288

[b] https://orcid.org/0009-0001-5010-7397

[c] https://orcid.org/0000-0001-7160-3026

[d] https://orcid.org/0000-0003-2571-5531

Filaments identified in the contra-rotating vortex zone persist in the stagnation zone and continue moving in the longitudinal direction, playing a key role in the interaction with wall flows (Gutmark et al., 1978). Furthermore, the counter-rotating filaments on either side of the jet's symmetry plane merge at the obstacle to form longitudinal rollers that cross this plane (Sakakibara et al., 2001).

This article proposes an open lightweight tool for airflow visualisation of PIV acquired data, only requiring a web browser. It aims at providing efficient particle and vortex tracking, displaying vortex centers and trajectories. More importantly, it estimates the vortex formation frequency, based on the captured image flow. Our contributions proposed in this article are the following:

- A lightweight tool for analysing air flow images;
- A velocity vector fields visualisation;
- A particle tracking system, with trajectories;
- A vortex tracking method, highlighting intensities and directions;
- A vortex apparition detection, related to the acoustic frequency.

In this paper, the visualisation system focuses on plane jets impinging on a slotted plate.

2 RELATED WORK

Visualising an airflow is particularly challenging since air is transparent to the naked eye. Alternative methods must be employed to highlight the flow patterns. Furthermore, the targeted phenomena often occur at high frequencies, difficult to capture or analyse in real time. Therefore, both high-speed visualisation techniques and advanced post-processing methods have to be implemented.

In many cases, PIV is used to track the movement of particles suspended in the air, allowing researchers to indirectly observe airflow behavior. Many tools already exist to visualise such complex data sets (Dorier et al., 2013; Ayachit et al., 2016; Sarton et al., 2023). Two major communities have formed around two key tools: ParaView (Ahrens et al., 2005; Ayachit et al., 2015) and VisIt (Kuhlen et al., 2011; Childs et al., 2012). They have been specifically designed for large-scale data visualisation, particularly well-suited for simulations. Despite their strengths, they are not versatile enough to accommodate experimental data provided by specific hardware.

Consequently, physicists often turn to commercial tools like DaVIS from LaVision, which are specifically tailored to handle experimental data (DaVIS, 2024). These tools are by design compatible with the associated hardware. However, in addition to their high cost, they are proprietary software, making adaptions to specific functionalities impossible.

As a result, many laboratories prefer to rely on custom-built solutions to process their data. They often use tools such as MATLAB, Octave, or Tecplot, for instance. The primary advantage of these solutions is that they allow complete control over the features developed, ensuring that the tools are tailored to meet the specific needs of physicists. However, the downside is that physicists may lack the programming expertise to develop fully optimised tools, leading to inefficiencies.

3 EXPERIMENTAL PLATFORM

When a plane jet reaches an obstacle, it produces an audible acoustic shock wave, that may interact with the plane jet, creating a self-sustained acoustic phenomenon. It is similar to the sound produced with wind instruments or to the howling wind in canyons for instance.

This article relies on an existing experimental setup that contains five main elements for studying air flows: a blowing system, an thin oil particles seeding system, a laser beam, a high frequency camera, and

an acoustic system. A full acquisition cycle can require up to a month of preparation for capturing one second of data. Figure 1 shows a photograph of the acquisition part of this setup.

Fluid flow patterns depend on various parameters, such as fluid viscosity, density, flow speed, and the geometric configuration of the medium. They are characterised by the Reynolds number (*Re*) (Sommerfeld, 1909; Bush, 2004). This value is thus fundamental when designing an experimental setup. A low Reynolds number corresponds to a laminar flow, while a high Reynolds number is related to a turbulent flow.

Figure 1: Photograph of the experimentation setup: (a) convergent nozzle, (b) slotted plate, (c) high-frequency cameras, (d) laser emitter, and (e) microphone.

Blowing System
First, the blowing system controls the flow velocity, directed toward a slotted plate. It comprises three elements:

1. A compressor and frequency chopper (Figure 2.a), located in an isolated room, that produces airflow while avoiding interference with acoustic phenomena from the impinging jet. A digital frequency chopper manages the motor frequency, controlling the jet's initial speed, which can reach 33 m/s (subsonic).

2. A $1m^3$ damping chamber and a tube with a convergent nozzle. It is equipped with three coarse metal meshes, reducing turbulence. The 1250 mm long rectangular tube (190 mm × 90 mm), fitted with honeycomb structures and a convergent noz-
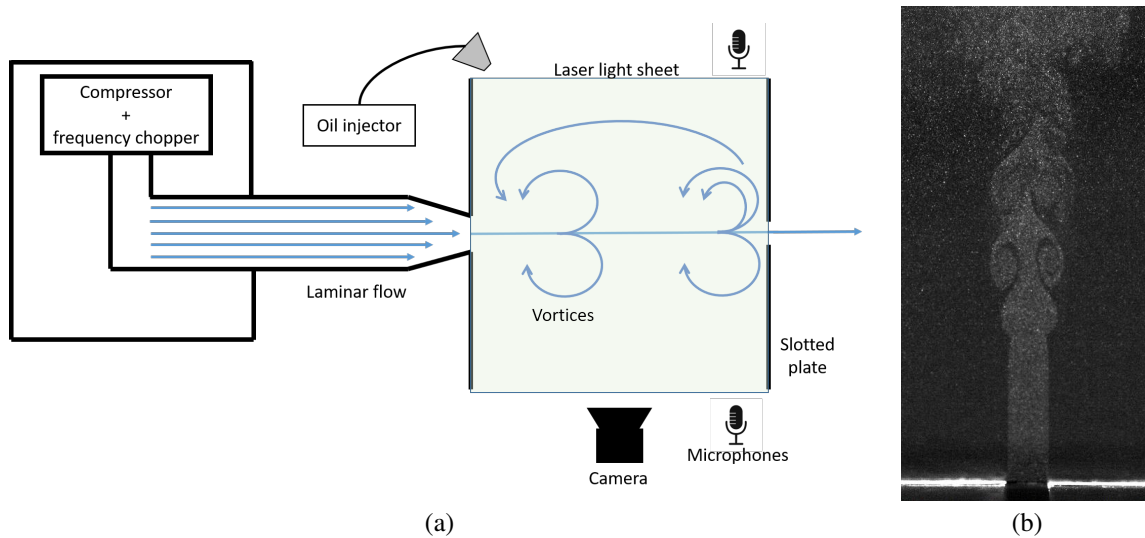
Figure 2: (a) Representation of the experimentation setup. On the left the compressor and frequency chopper generating the airflow outside of the experimentation room. In the middle the laminar flow. On the right the acquisition part. Oil particles are injected in the air flow and a high-frequency camera capture the response a of the light bouncing on the particles from a laser sheet. Finally, microphones captures the acoustic spectrum. (b) Raw Image produced for a free plane jet without any obstacle.

zle, produces a plane jet of height H=10 mm and width 190 mm, achieving an aspect ratio of 19. This ensures a laminar jet at the nozzle exit with minimal turbulence (Assoum et al., 2020).

3. An obstacle, corresponding to a 4 mm thick aluminum plate with a 45° beveled slot aligned to the nozzle outlet. Acoustic resonance occurs upon impact, and Reynolds number adjustments are controlled here. Image and acoustic acquisition are performed in this final element.

Image Acquisition

The fluid flow is seeded by thin oil particles, illuminated by a high-intensity pulse laser beam with short duration. The acquisition technique consists in capturing the resulting images at high frequency (at 3KHz for this article). The oil particles must be small enough to follow velocity gradients but large enough to scatter sufficient light, in order to minimize noise during processing. Seeding must be performed carefully, upstream from the measurement volume, for avoiding disturbances. Note that PIV measures particle velocity rather than exact flow velocity. For our experimentation, the camera is placed orthogonally to the laser plane. Synchronization and calibration ensure accurate data acquisition.

The system also includes an acoustic acquisition system, simultaneously with the image acquisition. 10 KHz Microphones are placed on each side of the experimentation setup capture the full acoustic spectrum. This article focuses on the visualisation system,

links between vortex analysis and acoustic effects will be considered in future work.

4 FLOW TRACKING

Studying the sound generated by a blowing system requires understanding the flow dynamics, and more specifically vortex formation. This is why we propose a tool for visualising air flow motion with its characteristics such as speed, transverse and longitudinal velocities, or vortex formation and motion. Our visualisation system uses as input the series of acquired images, each associated with its corresponding velocity vector field (Figure 2.b).

Input Data Direct Visualisation

Flow vectors are given as a set of 2D points aligned with a uniform grid in image space. Aligning these points with the acquired image at each time step allows for visualising raw data, with 3 modes: individual, transverse, and longitudinal velocities (Figure 3). A user-chosen colormap helps to visually identify regions of low or high velocities:

- The individual velocity mode (Figure 3.a) employs a mapping of the velocity vector norm, aiding shear flow analysis;
- The transverse mode (Figure 3.b) isolates the x-component of velocity, showing the extent of lateral motion;
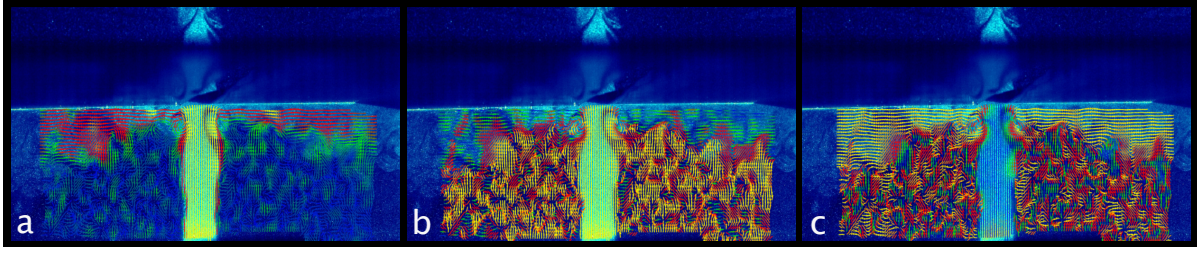
Figure 3: Visualisation of the vector fields, (a) individual velocity, (b) transverse velocity, and (c) longitudinal velocity, on top of the corresponding frame captured. Vector magnitudes are normalized and mapped on a predefined spectrum, that represents magnitudes: blue for low speed, green for intermediate, red for high, and yellow for the highest.

- The longitudinal mode (Figure 3.c) isolates the y-component of velocity, representing vertical motion, also highlighting upstream or downstream dynamics, useful for identifying rising or descending vortices.

Vortex Detection

Tracking vortexes can be managed using the Gamma 2 (Γ_2) criterion, proposed by (Graftieaux et al., 2001). It has successfully been employed for identifying vortices in turbulent flows. This approach differentiates between rotational and shear flows by integrating the local velocity field over a small domain. In rotation-dominated flows, particles move around a common center in a circular or spiral manner, indicating regions where the velocity field characterises coherent, organised rotational motion. The corresponding regions are referred to as vortices. Vortices are areas where fluid elements exhibit significant vorticity, a measure of the local rotation of fluid particles. In contrast, shear flows occur when fluid layers move parallel to each other at different velocities. In this case, no significant rotational movement of fluid elements occurs.

Γ_2 computations correspond to iterating through flow data and estimating vortex structures. They are later used to generate texture maps of vortex cores. The method mirrors the theoretical Γ_2 formulation, accurately distinguishing vortex cores from regions dominated by shear. Mathematically, Γ_2 expression at a point P is:

$$\Gamma_2 = \frac{1}{S} \int_S \frac{\overrightarrow{PM} \times (\overrightarrow{u}(M) - \overrightarrow{u}(P)) \cdot \overrightarrow{z}}{|\overrightarrow{PM}|^2} \, dS,$$

where S is the surrounding domain, $\overrightarrow{PM}$ is the vector from P to a neighbouring point M, and $\overrightarrow{u}(M)$ and $\overrightarrow{u}(P)$ represent the velocities at M and P. $\overrightarrow{z}$ is the unit normal vector to the observation plane. This computation highlights rotational flow regions, identifying vortices even in noisy environments.

In their work, (Graftieaux et al., 2001) compares two integration domains, square and circular, applied to the Γ_2 criterion. The conclusion is that circular domains generally offer better accuracy in detecting vortex cores by preserving the symmetry of the structures, while square domains, aligned with the Cartesian frame, simplify calculations and improve computational efficiency. In this implementation it makes more sense to use a square domain, as a core objective is to propose a visualisation at an interactive frame rate.

Vortex Trajectory Calculation

Proposing a viable vortex visualisation involves to recreate time coherence between the defined vortices throughout the source samples. Therefore, it tracks vortex trajectories by following particle movements through the flow field. The tracking is done by updating velocities and positions using bilinear interpolation.

At each time step, it computes particle velocities from the surrounding four grid points. The position update is computed as follows:

$$x_{\text{new}} = x_{\text{current}} + \frac{v_x}{K_v}$$
$$y_{\text{new}} = y_{\text{current}} + \frac{v_y}{K_v}$$

where v_x and v_y are the interpolated velocity components, K_v is a user-defined value employed for adjusting the search radius (a value of 3.0 is suitable in most cases). This step is repeated until the particle either exits the flow domain or its velocity approaches zero.
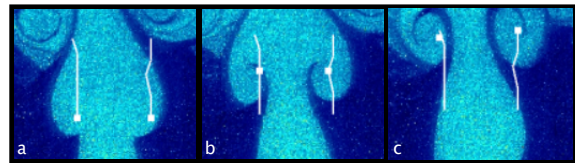

Figure 4: Vortex core trajectories and evolution of their positions over time.

Trajectories are computed at application start up and stored in memory. An interpolation process pro-

vides smoother approximations for each trajectory, lowering the variations due to noisy input data. Figure 4 illustrates the trajectory calculated for one vortex.

Wavefront Detection

We consider wavefronts as level sets, with scalar contours used to highlight threshold values. Vortex intensities (Γ_2) are used as input values. They outline regions of interest, where particle angular velocity indicates high rotational intensity, enabling the visualisation and tracking of vortex structures and velocity fronts in turbulent flows. They are integrated as precomputed textures. Transparency and intensity thresholds are dynamically adjustable, allowing flexible rendering over vector fields or vortex trajectories. This multimodal approach clearly depicts vortex boundaries by superposing level set contours on other flow features (Figure 5).
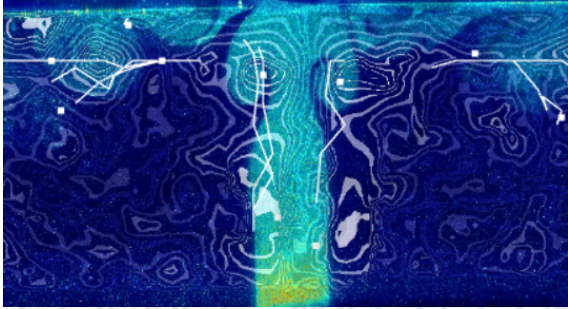

Figure 5: Multimodal visualisation of a single frame, present vortex cores with their trajectories and level set visualisation.

Vortex Frequency Calculation

Determining the frequency of vortex formation is also an interesting parameter in understanding flow dynamics, notably when linked with sound generation. For a given experimental setup, depending on the chosen *Re*, the acoustic phenomenon is directly related to the frequency of vortex formation. It is determined by counting the number of vortex cores detected over a series of frames.

The detection process relies on a rectangular region selected by the user (ax, ay) and (bx, by), mapped onto the data grid. The total number of detected vortex occurrences n, is divided by the time interval between frames, yielding the vortex frequency:

$$f = \frac{n}{\Delta t \times (j - i)},$$

where Δt is the time step between each frame of the acquisition, and $(j - i)$ represents the number of frames.

Implementation

The single most computationally expensive process concerns level sets (Γ_2). They are estimated in a preprocessing step, written in *python*, integrating the velocity field over localised regions and distributed (multi-thread operations) to enhance performance. This operation occurs only once per image series, ensuring all essential data is completely available in memory for real-time rendering.

Our real-time web-based tool relies on *javascript/webgl* for the interactive visualisation part. Adjusting vector colors for each mode is ensured with vertex and fragment shaders, enabling interactive visualisation of flow characteristics. Vortex trajectories are calculated interactively at run time, by tracking vortex cores across frames, from the input velocity field.

The system supports multiple visualisation modes (velocity, transverse, longitudinal), rendered in real-time based on user input. Multimodal visualisation allows users to switch between or combine modes dynamically, such as velocity fields, Γ_2 textures, and level set contours.

Additionally, vortex frequency in a user-specified region is calculated interactively by tracking vortex occurrences over time, relying on precomputed data and trajectory calculations.

5 RESULTS

Test System

Performance-wise, the tool was tested on a system equipped with an Intel i5 processor, an RTX 2060 laptop GPU, and 16GB of RAM, making it accessible to a broad audience with standard hardware. The tool operates entirely within a web browser, specifically Mozilla Firefox in our case, removing the need for specialised software installations.

Test Data

The dataset used for testing consists of airflow data captured over one second, with cameras recording at 3,000 frames per second, each dataset associated with a specific Reynolds number (Figure 6). Each series of acquisitions comprises 11GB of raw data and 8.9GB of computed data prepared for visualisation, including 3,000 images. Three datasets are presented in Figure 6 with an *Re* of 4700, 4800 and 5356 respectively. Variations in *Re* visually corresponds to variations of vortex core shapes and trajectories (note that higher *Re* does not necessarily imply higher vortex formation frequency). Our tool consistently delivers smooth

visualisation performance, with negligible impact on the fluidity of the rendering process.

Figure 2.b shows input raw data examples, they are grey-scale images associated with velocity vector fields. A look-up table enhances visualisation by highlighting particles in the flow, as shown in Figure 3, 4, and 7.

Vector Fields Visualisation

The generated velocity vector fields are presented in Figure 3. These vectors provide valuable insights into both rotation-dominated and shear-dominated regions. They reveal clear patterns of fluid rotation around vortex cores, enabling the identification of multiple vortices, their cores, and their trajectories, as well as tracking their evolution over time.

Multimodal Visualisation

Figure 7.a shows the captured camera image alongside the detected vortex cores in the current frame and their trajectories. Figure 7.b presents the Γ_2 values derived from the corresponding velocity vector field, providing a texture map that highlights regions dominated by rotational motion, making the vortex cores stand out more clearly. The colors represent the Γ_2 values and indicate the direction of vortex rotation, with saturated red and blue areas marking regions of intense rotational activity, confirming the presence of vortices while differentiating them from shear-dominated regions.

Figure 5, in turn, displays the level set visualisation based on the Γ_2 values, showing the scalar field of the flow and offering a qualitative measure of vortex intensity or strength. The level set contours provide an additional layer of insight, delineating regions of varying vortex intensity and tracking how these regions evolve spatially across the flow domain, as detailed in section 4. These contours also enable precise identification of velocity fronts during visualisation.

Together, these three images illustrate the strength of multimodal visualisation in fluid dynamics analysis. The camera image, the Γ_2 texture, and the level set, all together allow simultaneously observing the structure, intensity, and trajectory of vortices within the same simulation frame.

It is important to note that in multimodal visualisation, potential misalignment between images and velocity vectors must be considered. These misalignment may result from differences in timing or resolution across data sources. Therefore, a registration step, either performed in advance or dynamically, is necessary to ensure the visualised features align consistently.

Vortex Appearance Frequency

Figure 8 displays a user-selected area defined by points *a* and *b*, where the vortex frequency was calculated over a specified number of time steps in the simulation. Using the method described in section 4, and with an initial sampling rate of 5.1 kHz, the vortex appearance frequency was determined. In this region, the vortex trajectories revealed a frequency of 400 Hz, underscoring the periodic nature of vortex formation within the flow. The direct consequence of this information is that, considering such configuration, if it emits a noise, then its fundamental frequency will be at this given frequency.

Particle Visualisation

The tool offers a feature that allows for the visualisation of the movement of multiple particles, as demonstrated in Figure 9. Users can select particles in various ways: manually selecting a group of particles (a), isolating a single particle for detailed tracking (b), or selecting a group with a predefined shape (c). This flexibility enables users to analyse particle trajectories in different contexts.

It is particularly useful for comparing the movement of particles with that of vortex cores, providing deeper insight into how particles behave in rotation-dominated regions versus shear-dominated regions. By overlaying particle paths with vortex trajectories, it helps examining the interaction between the general flow and specific vortex structures, offering a comprehensive understanding of the dynamics within the flow field.

Discussion

The proposed system combines preprocessing and real-time components to enable a multimodal and interactive visualisation of flow dynamics. By using the Γ_2 criterion on velocity vector fields for vortex detection, the tool offers the ability to explore turbulent flow features in real time. The separation of computational tasks ensures that time-sensitive operations, such as vortex tracking and frequency computation, can occur interactively without compromising performance. Moreover, the vortex tracking algorithm relies heavily on the accuracy of the precomputed velocity fields, and any noise in the data may lead to inaccuracies in the trajectory visualisation. Although the system provides methods to smooth trajectories, future work could focus on improving trajectory interpolation techniques to further reduce the impact of noisy data.
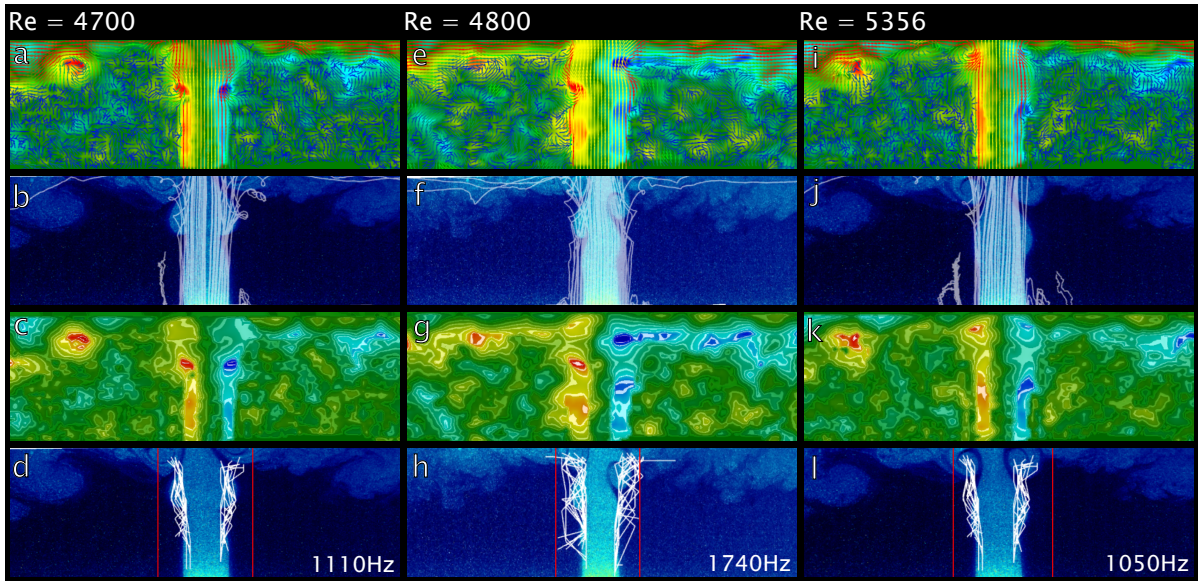
Figure 6: Multimodal visualisation of three datasets, corresponding to various Reynolds numbers, acquired with a sampling rate of 3kHz: (a, e, i) Γ_2 and vector fields ; (b, f, j) Frame capture and particle tracking; (c, g, k) Γ_2 and level sets; (d, h, l) Frame capture, vortex frequency calculation and resulting frequency.
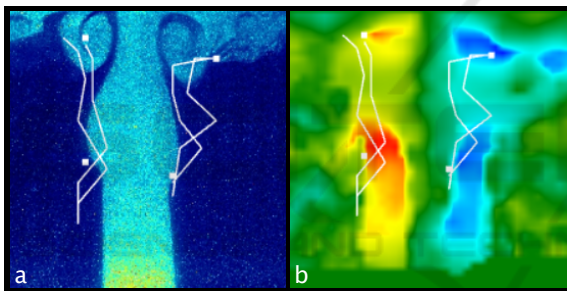

Figure 7: Multimodal visualisation of a single frame. (a) frame captures, vortex cores and trajectories; (b) Γ_2 texture, vortex cores and trajectories.

Figure 8: Vortex appearance frequency, for a given zone *ab* (red rectangle) and sampling frequency (slider). In white, all the vortex core trajectories passing through *ab*.

6 CONCLUSION

This article presents a lightweight, web-based visualisation system designed for tracking and analysing vortex dynamics in airflow experiments. It provides interactive tools for visualising flow velocity, vortex identification, and tracking by utilising high-frequency images and computed velocity vector fields. The system relies on the Γ_2 criterion to detect vortex cores and effectively differentiate between rotation-dominated and shear-dominated flow regions. It offers a multimodal visualisation approach by combining captured images, vortex trajectories, and level sets derived from Γ_2 values. This comprehensive view of flow dynamics enables users to observe interactions between vortices, track the evolution of flow patterns, and better understand the for-
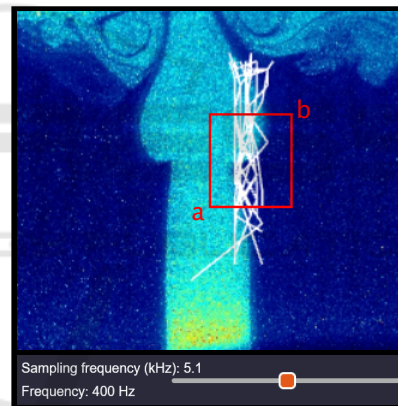
mation of acoustic phenomena. The inclusion of features such as vortex appearance frequency computation from selected regions further enhances the system's capacity to reveal intricate behaviors within the experimental setup.

Our system has smooth performance but results in a large memory footprint for extensive datasets. Future improvements consist in implementing real-time processing for specific calculations, reducing delays while maintaining interactivity during extended visualisations, or considering out-of-core techniques.

The current implementation uses Particle Image Velocimetry (PIV) data. Since the acquisition system is compatible with Stereo PIV setups (El Zohbi et al., 2024), with two spatially separated camera views, 3D
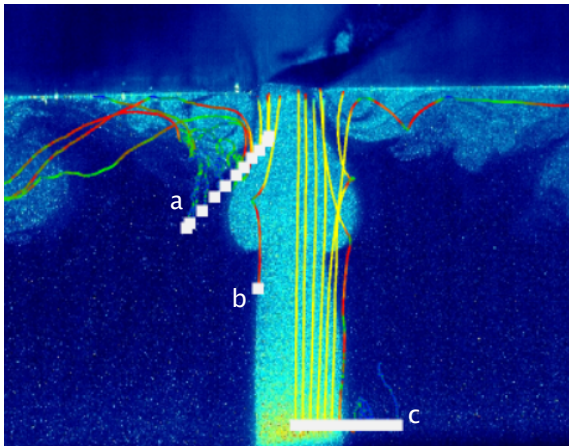
Figure 9: Visualisation of particles selected from the user interface: (b) single particle, (a,c) groups of particles.

visualisation becomes possible by registering datasets into a shared space. This would provide a more immersive view of flow phenomena, enhancing both visualisation and analysis.

Another interesting feature would be to compare flow predictions coming from simulations, to predict the acoustic effects generated by an experimental configuration. Such capabilities would enable physicists to predict noise production in advance, reducing costly trial-and-error experimentation and aiding in designing quieter, more efficient systems.

ACKNOWLEDGEMENTS

REFERENCES

Ahrens, J., Geveci, B., Law, C., Hansen, C., and Johnson, C. (2005). 36-paraview: An end-user tool for large-data visualization. *The Visualization Handbook*, 717:50038–1.

Assoum, H. H., Hamdi, J., El Hassan, M., Mrach, T., Abed Meraim, K., and Sakout, A. (2020). Energy transfers between aerodynamic and acoustic fields in a rectangular impinging jet. *Energy Reports*, 6:812–816.

Ayachit, U., Bauer, A., Geveci, B., O'Leary, P., Moreland, K., Fabian, N., and Mauldin, J. (2015). Paraview catalyst: Enabling in situ data analysis and visualization. In *Proceedings of the First Workshop on In Situ Infrastructures for Enabling Extreme-Scale Analysis and Visualization*, pages 25–29.

Ayachit, U., Whitlock, B., Wolf, M., Loring, B., Geveci, B., Lonie, D., and Bethel, E. W. (2016). The sensei generic in situ interface. In *2016 Second Workshop on In Situ Infrastructures for Enabling Extreme-Scale Analysis and Visualization (ISAV)*, pages 40–44. IEEE.

Bush, J. W. (2004). Surface tension module. *URL http://web.mit.edu/1.63/www/Lecnotes/Surfacetension*.

Childs, H., Brugger, E., Whitlock, B., Meredith, J., Ahern, S., Pugmire, D., Biagas, K., Miller, M., Harrison, C., Weber, G. H., et al. (2012). Visit: An end-user tool for visualizing and analyzing very large data.

DaVIS (2024). https://www.lavision.de/en/products/davis-software/.

Dorier, M., Sisneros, R., Peterka, T., Antoniu, G., and Semeraro, D. (2013). Damaris/viz: A nonintrusive, adaptable and user-friendly in situ visualization framework. In *2013 IEEE Symposium on Large-Scale Data Analysis and Visualization (LDAV)*, pages 67–75. IEEE.

El Zohbi, B., Assoum, H. H., Alkheir, M., Afyouni, N., Abed Meraim, K., Sakout, A., and El Hassan, M. (2024). Experimental investigation of the aeroacoustics of a rectangular jet impinging a slotted plate for different flow regimes. *Alexandria Engineering Journal*, 87:404–416.

Graftieaux, L., Michard, M., and Grosjean, N. (2001). Combining piv, pod and vortex identification algorithms for the study of unsteady turbulent swirling flows. *Measurement Science and Technology*, 12(9):1422.

Gutmark, E., Wolfshtein, M., and Wygnanski, I. (1978). The plane turbulent impinging jet. *Journal of Fluid Mechanics*, 88(4):737–756.

Kuhlen, T., Pajarola, R., and Zhou, K. (2011). Parallel in situ coupling of simulation with a fully featured visualization system. In *Proceedings of the 11th Eurographics Conference on Parallel Graphics and Visualization (EGPGV)*, volume 10, pages 101–109. Eurographics Association.

Sakakibara, J., Hishida, K., and Phillips, W. R. (2001). On the vortical structure in a plane impinging jet. *Journal of Fluid Mechanics*, 434:273–300.

Sarton, J., Zellmann, S., Demirci, S., Güdükbay, U., Alexandre-Barff, W., Lucas, L., Dischler, J.-M., Wesner, S., and Wald, I. (2023). State-of-the-art in large-scale volume visualization beyond structured data. In *Computer Graphics Forum*, volume 42, pages 491–515. Wiley Online Library.

Sommerfeld, A. (1909). Ein beitrag zur hydrodynamischen erklärung der turbulenten flüssigkeitsbewegungen. *International Congress of Mathematicians*, 3:116–124.

Yokobori, S., Kasagi, N., and Hirata, M. (1983). Transport phenomena at the stagnation region of a two-dimensional impinging jet. *Trans. JSME B*, 49(441):1029–1039.